PIV measurements of turbulent jets issuing from triangular and circular orifice plates

XU MinYi[1]*, ZHANG JianPeng[2], MI JianChun[2], NATHAN G J[3] & KALT P A M[3]

[1] *Marine Engineering College, Dalian Maritime University, Dalian 116026, China;*
[2] *State Key Laboratory of Turbulence & Complex Systems, College of Engineering, Peking University, Beijing 100871, China;*
[3] *Centre for Energy Technology and School of Mechanical Engineering, University of Adelaide, SA 5005, Australia*

The present study experimentally investigated the near-field flow mixing characteristics of two turbulent jets issuing from equilateral triangular and circular orifice plates into effectively unbounded surroundings, respectively. Planar particle image velocimetry (PIV) was applied to measure the velocity field at the same Reynolds number of Re=50,000, where $Re = U_e D_e / \nu$ with U_e being the exit bulk velocity and ν the kinematic viscosity of fluid, D_e the equivalent diameters. The instantaneous velocity, mean velocity, Reynolds stresses were obtained. From the mean velocity field, the centreline velocity decay rate and half-velocity width were derived. Comparing the mixing characteristics of the two jets, it is found that the triangular jet has a faster mixing rate than the circular counterpart. The triangular jet entrainments with the ambient fluid at a higher rate in the near field. This is evidenced by a shorter unmixed core, faster Reynolds stress and centreline turbulence intensity growth. The primary coherent structures in the near field are found to break down more rapidly in the triangular jet as compared to the circular jet. Over the entire measurement region, the triangular jet maintained a higher rate of decay and spread. Moreover, all components of Reynolds stress of the triangular jet appear to reach their peaks earlier, and then decay more rapidly than those of the circular jet. In addition, the axis-switching phenomenon is observed in the triangular jet.

triangular jet, turbulent mixing, coherent structures, axis-switching

PACS number(s): 47.27.wg, 47.80.Cb, 47.85.lk

1 Introduction

Largely because of their more effective mixing with ambient fluid than comparable circular jets, noncircular jets have been extensively investigated in the past three decades [1–22]. It is found that the increased mixing capability of such noncircular jets is related either to instabilities induced by the sharp corners of non-circular nozzles through the asymmetric distribution of mean flow field and pressure, or to the non-uniform curvature of the initial perimeter [1]. It

is thought that both factors can increase the three-dimensionality of the jet flow structures, which results in entrainment enhancement. For corner-containing configurations (for example, triangular or rectangular nozzle), the corners can promote the formation of fine-scale vertical structures and thus enhance fine-scale turbulence [3,4]. For jets whose aspect ratio >1 (e.g., rectangular or elliptic jets), the azimuthal curvature variation produces three-dimensional vertical structures and non-uniform self-induction. As a result, these non-circular jet flows entrainments with surrounding fluid are more rapid in the direction of the minor axis of their nozzle exit than that of major axis. Thus, as these jet flows develop downstream at a certain distance from the

*Corresponding author (email: xuminyi@dlmu.edu.cn)

nozzle exit, the cross-section of the mean flow appears to alter the minor axis and major axis [1,2]. This phenomena of noncircular jets are called "axis-switching", also being evidenced in a number of numerical simulation studies [5,6].

In the case of triangular free jets, previous experimental investigations were conducted using conventional point by point measurement techniques, such as hot-wire anemometry (HWA) [7–9] or laser Doppler velocimetry (LDV) [10]. Based on his hot-wire measurements of triangular jets, Quinn [7,8] obtained the mean streamwise vorticity, half-velocity width and turbulent kinetic energy, and found that near-field mixing in the triangular jet is faster than in the circular jet. The axis-switching phenomenon in Quinn's experiment [7,8] occurred at x/D_e=5, where D_e is the equivalent diameter. Similarly, Mi and Nathan [9] experimentally showed the centreline velocity characteristics of turbulent free jets issuing from nine different shaped nozzles including triangular nozzle using HWA. The work of Mi and Nathan [9] shows that the lack of axisymmetry at the nozzle exit generally increases the overall entrainment in the near field, which was indicated by the faster decaying mean velocity, and the growing fluctuating intensity. However, at sufficiently downstream from the exit, there are insignificant differences occurring in the probability density functions (PDF) of the mean velocity of the jet, as well as in the Taylor and Kolmogorov micro-scales. With LDV measurements of free jets issuing from five different shaped nozzles, including triangular, smooth pie, contraction circular, rectangular, and square, Iyogun and Birouk [10] observed that that triangular jet exhibits the highest entrainment and spread rate among the five nozzles. In addition, it was demonstrated that the use of sudden expansion can further improve the entrainment and spread rates of jet flows.

However, the single point measurement techniques cannot provide spatially correlated velocity, thus vortical structures information cannot be shown. Moreover, the HWA technique has poor accuracy in flow regions, where highly three-dimensional vortical structures and great turbulent intensity are contained [11–14], such as the shear layer and near field flow region. Therefore, we performed the measurements of velocity for a triangular jet and a counterpart circular jet using PIV. Different from the HWA technique, the accuracy of the PIV technique is not significantly influenced by flow three-dimensionality or high turbulent intensity since PIV technique is almost interference-free relative to the flow. Therefore, PIV becomes critical technique to study different types of turbulent flows [15–19]. In particular, the PIV can measure a planar field of instantaneous velocity concurrently, and thus the vertical structures can be provided in timely manner [11].

To further investigate on the turbulent mixing characteristics of triangular jets in the development region and provide more experimental results for triangular jets in the literature, the present study conducted PIV measurements of two jets respectively issuing from a equilateral-triangular orifice and a circular orifice. Under the identical rigs and Reynolds number, the two jets have identical nominal inflow boundary conditions. The instantaneous velocity field, streamlines, mean velocity, and turbulence Reynolds stresses are reported for quantifying the differences between the triangular jet and circular jet. Also, these results can be used for future fundamental studies in jet flow.

2 Experimental details

As the present experiments were conducted at the University of Adelaide using similar setup as detailed in Mi et al. [11], only a brief description is provided here. Figure 1 shows the circular and triangular orifice plate, and their dimensions. These two orifice plates have the same opening area (A) and thus the identical equivalent diameter D_e [$\equiv 2(A\pi^{-1})^{1/2}$] of approximately 12 mm.

In Figure 2, the arrangement of the PIV measurement system is presented. This rig is positioned vertically under a 1.5 m×1.5 m extraction hood located 2 m above the ground and 800 mm above the nozzle exit. The hood is applied to
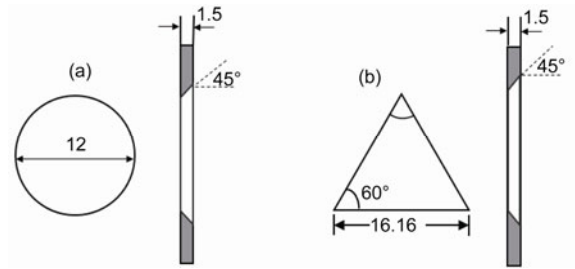
Figure 1 Present orifice shapes and dimensions (mm). (a) Circle: D_e =12 mm. (b) Triangular: D_e = 12 mm.
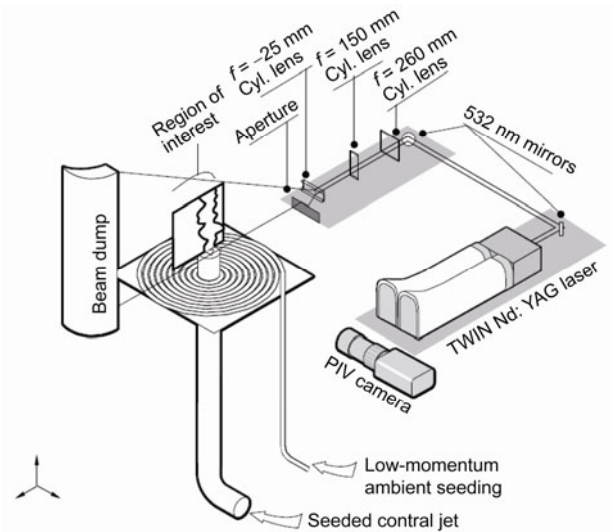
Figure 2 Experimental arrangements of the PIV system and the coordinate system [11].

collect the olive oil droplets, which is used to seed the jet flow. The conditioned air is supplied by a compressor with an operating pressure of up to 650 kPa. The supply tube which has a constant cross-section of 25.4 mm I.D and 1000 mm in length, is attached to an orifice plate.

The flow rate through the tube was metered by a pressure gauge and a Fisher and Porter tri-flat flow meter, which located at about 6 inner-diameters of the tube upstream of the exit. The mean velocity profiles at the exit of the tube exhibited good axial symmetry, but not adhering to the one-seventh power-law (see Figure 3 of Mi et al. [11]). This indicates that the flow out of the tube was not fully developed. The triangular and circular jets were measured at the same Reynolds number of $Re = U_eD_e/v = 50,000$, where U_e is the exit bulk velocity and v is the kinematic viscosity of fluid. In addition, the streamwise turbulence intensity was about 3% at the center and up to 26% near to the tube wall.

The velocity measurements were conducted using particle image velocimetry, PIV, realised by a Quantel Brilliant Twins double-head Nd:YAG laser at a frequency of 10 Hz and power of 250 mJ per pulse at $\lambda = 532$ nm. Depending on the flow velocity field, the temporal separation between laser pulses was adjusted from 10 to 40 μs. Through the cylindrical and spherical lens, the pulse laser is rendered a light sheet, whose thickness was about 1 mm. Then, a CCD camera was used to shoot the images of tracer particles in the flow field within the light sheet. The camera images were recorded in pairs and each image of the pair was taken at respective exposure. The MegaPlus ES1.0 camera was operated in triggered double exposure mode, with a 1008×1018 pixel array. The collection optics comprised a Nikon ED 70–300 mm telephoto lens coupled to the camera C-mount with an adapter. The measurement imaging region was 100 mm×100 mm, so that each pixel images approximately 100 μm in each direction. The time delay between laser pulses was selected so that the interrogation region could be set to 32×32 pixels, with 50% offset. This resulted in an effective resolution for the velocity measurements of 3 mm×3 mm. Relative to the camera and laser sheet, the nozzle was translated once to measure a greater flow region, which covers the axial region $0 < x < 16D_e$, with x being the downstream distance from the orifice plate (upstream side, see Figure 1).

The entire dataset of PIV image pairs were saved for post processing. The instantaneous velocity field was obtained from the cross-correlation of each image pair. From an ensemble of 500 instantaneous velocity fields, the velocity statistics (mean velocity, Reynolds stresses) were obtained for each jet. As reported in Mi et al [11], the independence of all derived velocity statistics from the ensemble size was confirmed by ensemble down-sampling. The derived mean field achieved statistical convergence with an ensemble size larger than 40–50 images, while turbulence Reynolds stresses became statistical convergence for ensembles greater than 200–250 images. The experimental errors for the measured quantities were estimated. The various statistics obtained around the mean velocity half-width at $x/D_e = 8$ were as follows, that is, the mean axial velocity $[U] \approx \pm 1.5\%$; the RMS velocities $[\langle u^2 \rangle^{1/2}] \approx \pm 2.5\%$ and $[\langle v^2 \rangle^{1/2}] \approx \pm 2.6\%$. In addition, the influence of spatial resolution on the mean and RMS results were confirmed by the progressive coarsening of the resolution from 2.6 mm×2.6 mm to 9.4 mm×9.4 mm. The results were demonstrated by Figure 4 in Mi et al. [11]. It was found that the influence of this coarsening was negligible for $x/D_e > 6$. Importantly, there was no significant effect of this coarsening on mean and RMS results around the centerline throughout the entire dataset.

3 Results and discussion

3.1 The instantaneous velocity field

Figures 3(a)–(c) show typical instantaneous velocity vectors (black arrows) and velocity magnitude contours (colored) at $x/D_e \leqslant 8.2$ for the free triangular jet (Figures 3(a) and (b)) and circular jet (Figure 3(c)) of investigation. The instantaneous velocity field is normalized by the mean velocity at the centre of nozzle exit plane, U_m. The x-y and x-z planes of the triangular jet are corresponding to the asymmetric and symmetric planes, respectively. Figures 3(a)–(c) clearly demonstrated that the column of the jet performs with an oscillating manner. In addition, the velocity contours in the central regions are high but discontinuous. This reflects the features of entrainment and interactions with the surrounding fluid by large-scale vortical structures in the shear layers. Also, the length of the high velocity (red) in triangular jet is shorter than that of circular jet, which is expected because of the higher entrainment and decaying rate of the triangular jet with ambient fluid than the circular jet.

To reveal the coherent structures in the jet shear layers, the corresponding streamlines of the instantaneous flow fields are obtained by translating the reference frame at a speed of $0.6U_e$ for both jets. The translating speed was selected based on Hussain and Clark [22], which showed that the large-scale vortical structures in the near field of the circular jet translate downstream at about $0.6U_e$. The sensitivity of the streamlines was confirmed by using differing translating velocities and no significant difference was observed. Thus, the instantaneous streamlines together with vorticity contours were obtained using this method, as shown in Figure 4. It is obvious to find that the streamlines is consistent with vorticity contours. Therefore, the present method is useful to reveal the underling structures.

The large scale vortical structures are clearly identifiable over the range approximately $1 \leqslant x/D_e \leqslant 5$ in the triangular jet (Figures 4(a) and (b)) and $1 \leqslant x/D_e \leqslant 7$ in the circular jet (Figure 4(c)). Originating from the rolling up of the initial shear layers, these vortical structures are believed to dominate the
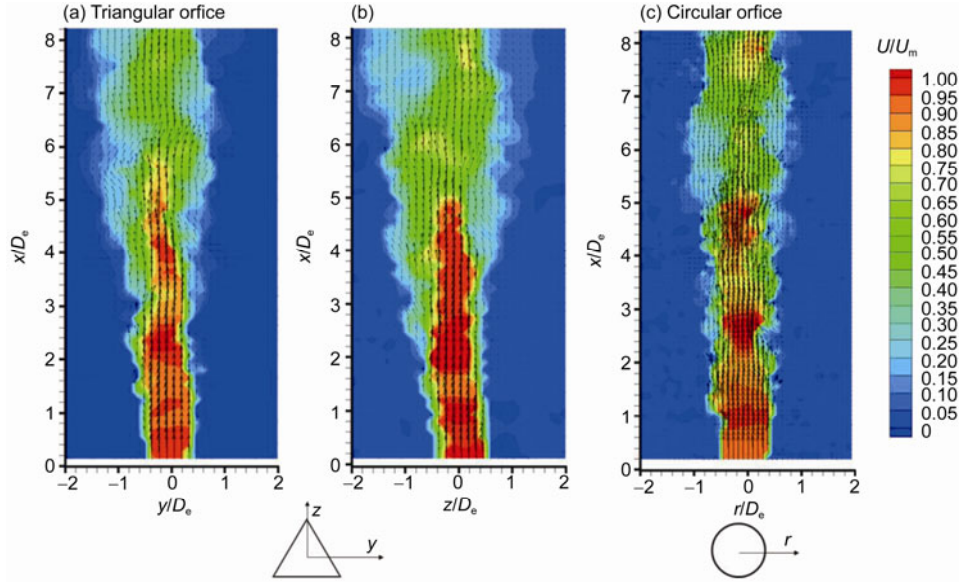
Figure 3 Typical instantaneous velocity vectors, contours in (a) and (b) the *x-y* and *x-z* planes of the triangular jet and (c) the central plane of the circular jet.
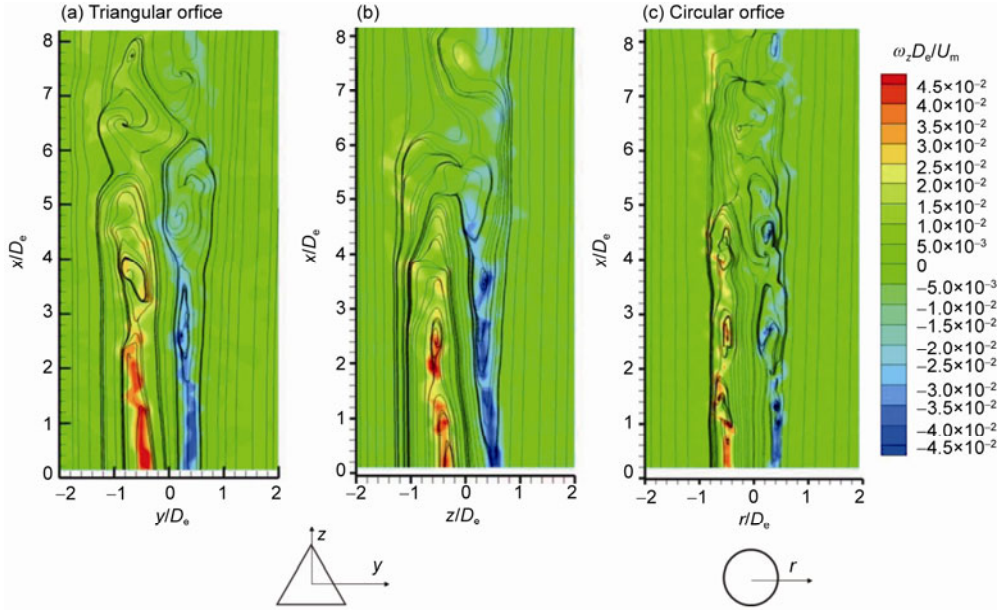
Figure 4 Typical instantaneous streamlines in (a)–(c) in the coordinate system translating at a speed of $0.6U_e$ for the two OP jets. Also shown are the *z*-component vorticity contours, whose magnitude is shown in the color scale.

entrainment with ambient fluid and initial growth in jets [5]. In the circular jet (Figure 4(c)), it clearly shows that the primary vortical structures grow by pairing. Compared to the circular jet, in the triangular jet (Figures 4(a) and (b)), these large-scale structures are more three-dimensional. Particularly, in the *x-z* plane of the triangular jet (Figure 4(b)), the vortical structures near the bottom part ($z/D_e<0$) seem larger than that of sharp corner part ($z/D_e>0$). This indicates that the corner can induce small-scale vortical structures, thus increase the small-scale turbulent mixing. However, the bottom can promote large-scale flow struc-

tures, which appear to be the dominant fluid-dynamic process involved in the entrainment of the triangular jet with ambient fluid. The difference of vortical structures between triangular jet and circular jet also suggests that the jet entrainment rate may be higher in the former than the latter. The downstream propagation of the flow structures in both jets is evident throughout the images. The structures for both jets are complex and hence it is not possible to identify a single vortex core. This reveals that the large-scale vortical structures in downstream development for both jets are three-dimensional.

Although large-scale vortical structures existing in the initial region for both jets, there is a critical difference between the triangular and the circular flows. The sharp corners of the triangular orifice can increase the instability of the initial shear layer. Hence, the flow structures in the triangular jet are always three-dimensionality. Conversely, the circular orifice can ensure axisymmetry at the nozzle exit plane, which results in the presence of the pairing vortical structures in the initial region. As the flow developing downstream, the vortical structures in circular jet become increasingly three-dimensional.

Figures 3 and 4 appear to show the fundamental difference between underlying vortical structures of the jets. It can be noted that the initial large-scale vortical structures of the triangular jet are more three-dimensional that that in circular jet. While the circular jet spreads downstream and mixes with ambient fluid, the spreading and mixing rates seem to be lower than those of the triangular jet. Support for this observation can be obtained indirectly from the instantaneous velocity (red color for the highest contour) decay which is more rapid in the triangular case as the flow proceeds downstream. The differences in spreading and decaying (and thus entrainment) between the two jets are quanti-

fied below by the mean velocity.

3.2 The mean velocity field

Figures 5(a) and (b) present the normalised mean velocity (U/U_m) contours in the two characteristic planes of the triangular jet, that is, the x-y plane and x-z plane. Comparably, the normalized mean velocity through the central plane of the circular jet is shown in Figure 5(c). These measurement regions cover the near-field over the range $0.1 \leqslant x/D_e \leqslant 16$. Also shown (dashed lines) is the locus of the mean-velocity half-width Ψ_{hw}, at which the mean velocity is a half of the centreline velocity, that is, $U = 0.5U_c$.

Thus, the significant differences between the mean velocity fields of the triangular jet and circular jet are revealed in Figures 5(a)–(c). In the x-z plane of the triangular jet (Figure 5(b)), the mean velocity contours are asymmetry in the region of $x/D_e=0$–10, which is also evidenced by the half-width line Ψ_{hw}. The main jet spreading out from the exit plane to $x/D_e \approx 3$ bends towards the flat side ($x/D_e<0$) from the corner side ($x/D_e>0$) and then returns to the centreline. The force causing such phenomenon is the lower pressure resulting from the larger scale vortical structures in the
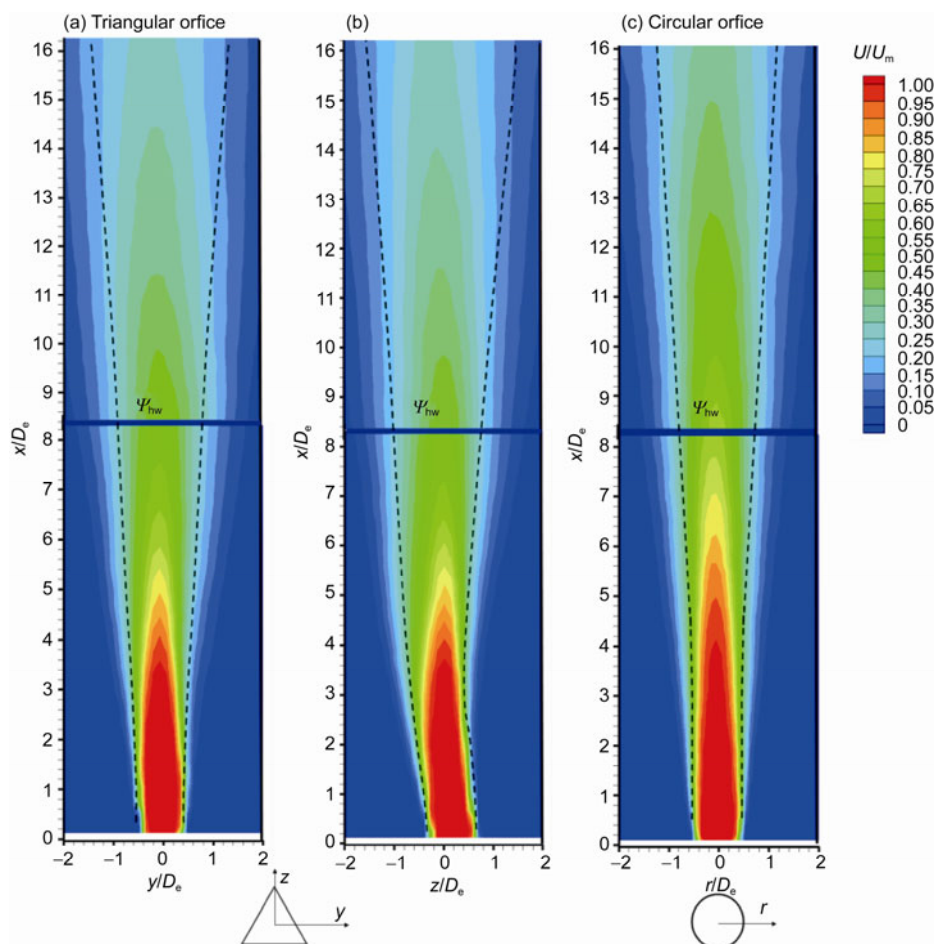
Figure 5 Normalised mean velocity (U/U_m) contours in (a) and (b) the x-y and x-z planes of the triangular jet and (c) the central plane of the circular jet.

flat side (x/D_e<0). But as these large-sale structures stretch and break, they gradually become smaller scale. Interestingly, there is a position where half-width in the flat side equals to the corner side in the region of 1<x/D_e<2. This can be better observed and qualified below in Figure 7. Such phenomenon is called "axis-switching", which is considered to be one of critical factors for non-circular jets to have more effective mixing performance than comparable circular jets [3,4,20,21,23–26].

However, with increasing downstream distance from the nozzle, the mean velocity contours and the half-width line Ψ_{hw} in the x-z plane seems to be symmetry. In addition, the evolution of the mean velocity in both x-z plane and x-y plane is nearly identical with each other in the region of x/D_e>10. It indicates that downstream flow gradually becomes symmetry as large-scale vortical structures beak down into small-scale turbulence by the entrainment with ambient fluid and the interactions with each other.

As both jets proceed downstream, it appears that the circular jet spreads out at a lower rate than the triangular jet. In addition, the high mean velocity (red contours) of the triangular jet decays more rapidly than the circular jet. Thus, the triangular jet spreads and decays at a higher rate than the circular jet, which implies a larger rate of entrainment of ambient fluid.

More evidence to support the above observation can be found in the Figures 6 and 7, which shows centreline variations of the normalized streamwise velocity and half-velocity widths, respectively. The magnitudes of centreline velocity and half-widths reflect the decay and spread rates of jet flows. Over the range of 0.1≤x/D_e<16, we extracted the data reported in Figures 6 and 7 from the PIV measurements. Also, Figure 6 includes the hot-wire measurements of U_m/U_c for a triangular jet by the data of Mi and Nathan [9] at Re≈1.5×10^4 with the same experimental configuration and the data of Quinn [7] at Re≈20.8×10^4 with different experimental configuration.

Clearly, Figure 6 reveals that the triangular jet decays faster than the circular jet over the range of 0.1≤x/D_e<16. Also, the length of "unmixed core" L_{pc} (defined as the location at which U_m/U_c≈1.01) of the triangular jet is shorter than that of the circular jet, with L_{pc}≈2.8D_e and L_{pc}≈3.5D_e, respectively. This shows that the triangular jet mixes with surroundings more effectively than the circular jet.

The mean velocity of the triangular jet measured by Mi and Nathan [9] decays faster than the present PIV result (see Figure 7 and Table 1). This may be as a result from the effect of Reynolds number. Du et al. [27] and Deo et al. [28] studied the effect of Reynolds number on round jet and plane jet, respectively. Both groups found that the decay rate decreases as Reynolds number increasing until to a critical Reynolds number, after which the decay rate becomes a constant. For round and plane jets, the critical Reynolds numbers are both about 10,000 which is defined
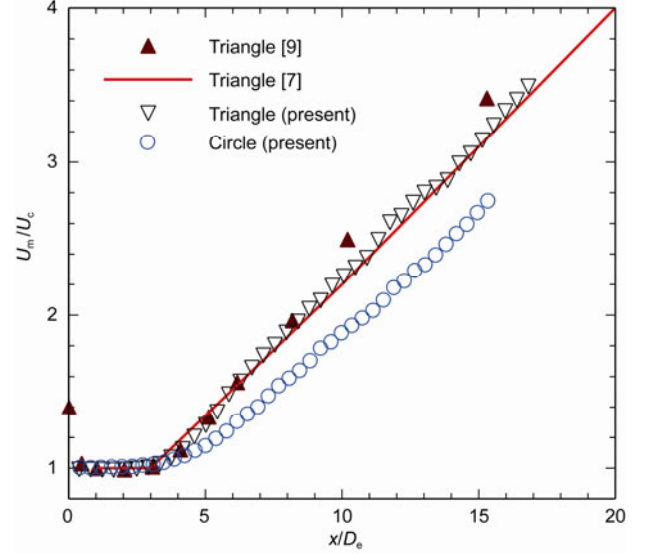
Figure 6   (Color online) Mean velocity decay along the jet centreline.
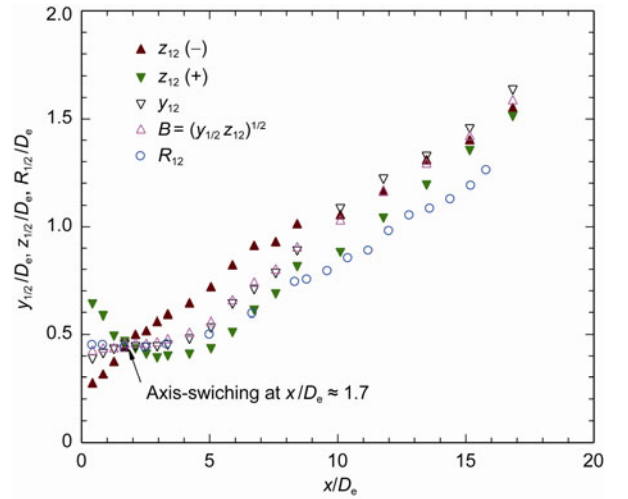
Figure 7   (Color online) Half-velocity widths of the triangular jet in comparison with the circular counterpart.

by the diameter of the exit nozzle and the exit mean bulk velocity. However, recently, Xu et al. [29] investigated the influence of Reynolds number on square jets and found that the critical Reynolds number is about 30,000. This suggests that the critical Reynolds number is not universal for different types of jets. The exit Reynolds number of the triangular jet [9] and the present triangular jet increases from 1.5×10^4 to 5×10^4. Correspondingly, the decay rate decreases from 0.203 to 0.018. This suggests that the critical Reynolds number for triangular jets should be larger than 1.5×10^4.

It can be noted that the centreline mean velocity for the triangular jet differs significantly with the earlier hot-wire measurements of Quinn [7] in the region of x/D_e<10. Particularly, the "unmixed core" of the triangular jet is longer as reported elsewhere [7]. This discrepancy is associated with different upstream flow conditions. Compared to the

present study using triangular orifice plate, Quinn [7] adopted sharp-edged triangular orifice, and hence achieved a low turbulent intensity upstream flow condition. However, the present data agrees well with results [7] in the region of $x/D_e > 10$. This suggests that the difference between two triangular in the near field can gradually disappear as flow developing downstream for high Reynolds number (The Reynolds number of the present and Quinn [7] triangular jet are, 5×10^4, 20.8×10^4, respectively). Hence, it suggests that the critical Reynolds number for triangular jets is smaller than 5×10^4. In addition, it is worth investigating the influence of Reynolds number on triangular jets with the same configuration and measurement technique.

Figure 7 clearly shows that the half-velocity widths of the triangular, including $y_{1/2}$, $z_{1/2}(-)$, $z_{1/2}(+)$, and half-velocity equivalent radius $B=(y_{1/2} z_{1/2})^{1/2}$, are larger than the half-velocity radius $R_{1/2}$ of the circular jet. This indicates that the triangular jet spreads faster than the circular jet, which is consistent with the higher decay rate observed in Figure 6. In addition, the differences of half-velocity widths between the triangular jet and the circular jet further provide that the former jet entrains with surrounding more rapidly than the latter.

Also, Figure 7 presents the "axis-switching" phenomenon for the triangular jet at $x \approx 1.7 D_e$. Because of the asymmetry of mean velocity in the x-z plane (Figure 5(b)), there are two velocity half-widths, that is, $z_{1/2}(-)$ and $z_{1/2}(+)$ being the half-widths in the flat side ($z/D_e < 0$) and the corner side ($z/D_e > 0$), respectively. From Figure 7, it shows that $z_{1/2}(+)$ decreases quickly from the exit plane to $x \approx 3 D_e$, and then increases as flow developing downstream. Comparably, $z_{1/2}(-)$ continuously increases. There is a critical position ($x=1.7 D_e$), where the $z_{1/2}(-)=z_{1/2}(+)$. The phenomenon is termed "axis-switching". Note that, two mechanisms were identified to govern the axis-switching phenomenon [4]. The initial mechanism is that a roll-up azimuthal vortical structures can induce velocities. The other mechanism is that streamwise vortical pairs can induce velocities [2]. The vortical structures near corner portions of a triangular nozzle move ahead faster than that near the flat portions, thus the large-scale vortical structures near the flat portions become small-scale. After several rotations, the vortical structures become somewhat disturbed, with the asymmetry in the x-z plane gradually become symmetrical as the jet proceeds downstream, as shown in Figure 5(b). These contortions can be attributed to the growth of azimuthal vortex instabilities [30].

From Figures 6 and 7, it appears that the self-similarity relations of centreline mean velocity and half-velocity width, that is, $U_m/U_c \sim x$ and $R_{1/2} \sim x$, are approximately valid for $x/D_e \geqslant 8$ in the circular jet, but not for the triangular jet over the entire measurement region. However, it is unnecessary for the mean flow achieve self-similarity when the two relations satisfy. To achieve self-similarity, it requires that the lateral normalized profiles of the mean velocity by the cen-

treline value at all the downstream positions collapse into each other, that is, $U/U_c=f(\eta)$, with η being the later distance from the centreline, normalized by half-widths as $r/R_{1/2}$, $y/y_{1/2}$ or $z/z_{1/2}$. Note that, in the x-z plane of the triangular jet, $\eta = z/z_{1/2}(-)$ is in the flat side, and $\eta = z/z_{1/2}(+)$ is in the corner side. These profiles are shown in Figure 8, which also includes the far-field mean velocity profile obtained by Hussein et al. [31] for a smooth contraction circular jet and the Gaussian distribution $U/U_c=\exp(-\eta^2/2)/(2\pi)^{1/2}$. It is surprising to find that the later mean velocity profiles for the present circular jet collapse well into each other for $x/D_e \geqslant 10$, which can induce that the mean flow of the circular jet approximately achieve a self-similar state for $x/D_e \geqslant 10$, together with the centreline mean velocity and half-velocity widths following their self-similarity relations. In addition,
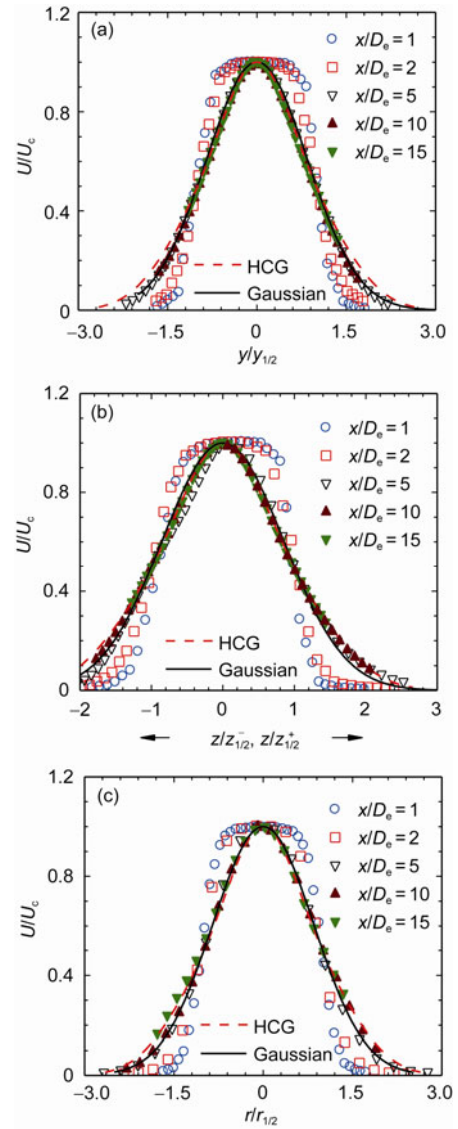
Figure 8 (Color online) Lateral profiles of the normalized mean velocity (U/U_c) in (a) and (b) the x-y plane and x-z plane of the triangular jet and (c) the central plane of the circular jet.

Figure 8(c) presents that the self-similar mean velocity profiles of the circular jet collapse well between Gaussian and Hussein et al. [31]. This indicates that the inflow conditions has little affect on the mean flow field. As shown in Figure 8(a), the later profiles of the mean velocity in the x-y plane of the triangular jet seem to follow the Gaussian distribution for $x/D_e \geqslant 10$. Also, a similar trend occurs in the x-z plane (Figure 8 (b)), where the later distance from the centreline is normalized by different half-widths, that is, $\eta = z/z_{1/2}(-)$ for $z/D_e < 0$, and $\eta = z/z_{1/2}(+)$ for $z/D_e > 0$. However, the mean flow of the triangular jet is not axisymmetric, which is evidenced by the half-widths of the triangular jet which do not equal each other in the entire measurement region (Figure 7).

3.3 The fluctuating velocity field

Figures 9–11 show contours of the Reynolds normal and shear stresses normalized by the maximum velocity U_m, that is, $\langle u^2 \rangle / U_m^2$, $\langle v^2 \rangle / U_m^2$ and $\langle uv \rangle / U_m^2$ in the xy plane and $\langle u^2 \rangle / U_m^2$, $\langle w^2 \rangle / U_m^2$ and $\langle uw \rangle / U_m^2$ in the xz plane of the triangular jet and in the central plane of the circular jet, for $x/D_e \leqslant 16$. The half-width locus, Ψ_{hw}, is shown as a reference. Also, it can be noted that the relatively poor PIV resolution in the jet near field caused discontinuous contours of the Reynolds stresses, particularly for $\langle v^2 \rangle$ and $\langle w^2 \rangle$ at $x/D_e < 3$.

From these plots, several observations can be made.

Firstly, the highest values of $\langle u^2 \rangle / U_m^2$ are consistently located near the half-widths in both the xy and xz planes for the triangular jet (Figures 9(a) and (b)), and near the half-radius for the circular jet (Figure 9(c)), while the corresponding locations for $\langle u^2 \rangle / U_m^2$ and $\langle u^2 \rangle / U_m^2$ shift inward away from Ψ_{hw} and arrive at the axis at $x/D_e > 4$–5 for the triangular jet and $x/D_e > 5$–6 for the circular jet (Figures 10(a)–(c)). The difference results from the breakdown of large-scale vortical structures, which causes the values of $\langle u^2 \rangle / U_m^2$ and $\langle u^2 \rangle / U_m^2$ to increase rapidly. As shown in the typical instantaneous streamlines (Figure 4), the large-scale vortical structures of the triangular jet breakdown earlier than those of the circular jet. Secondly, the absolute value of the shear stress in both jets reaches the maximal value approximately Ψ_{hw} in the near field, and the maximum shifts inward farther downstream in both measurement planes. The above behaviours of the Reynolds normal and shear stresses are associated with the mean shears ($\partial U / \partial y$ and $\partial U / \partial z$) whose maxima are located around the half-widths in the near field but move to an inner location at $y \approx 0.8y_{1/2}$ or $z \approx 0.8z_{1/2}$ at $x/D_e > 10$. Therefore, both the jet half-widths and maximal Reynolds stresses occur at the maximal mean shears, regardless of turbulent jets generated from any typed or shaped nozzles. In addition, as flow developing downstream from the exit plane, all components of Reynolds stress of the triangular jet appear to reach the peaks earlier
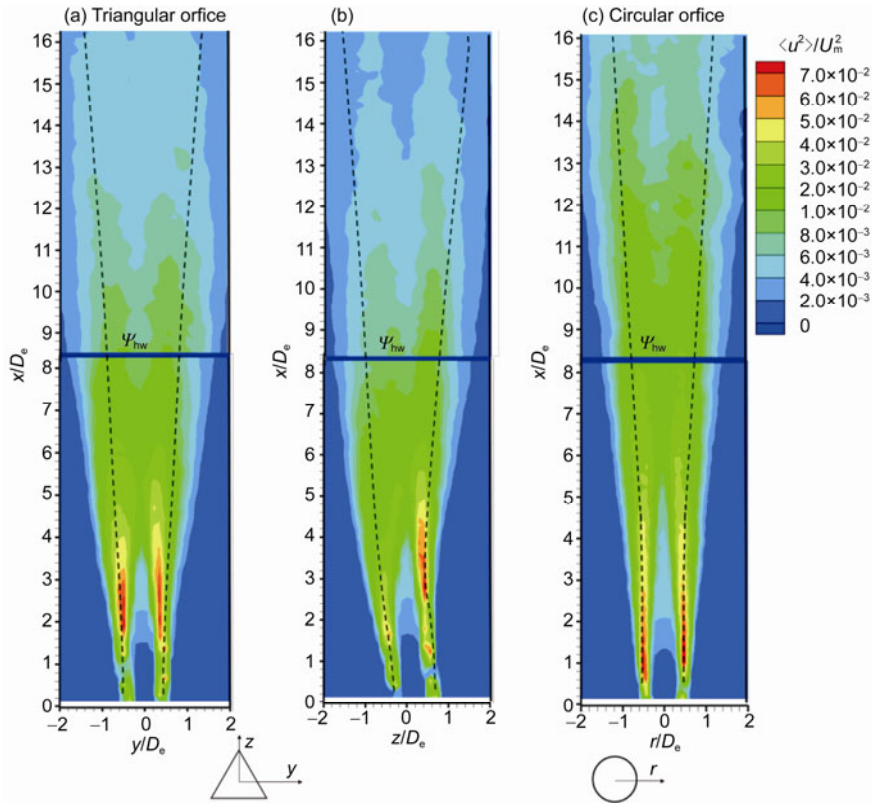
Figure 9 Contours of the streamwise component of the normal stress ($\langle u^2 \rangle / U_m^2$) in (a) and (b) the x-y and x-z planes of the triangular jet and (c) the central plane of the circular jet.
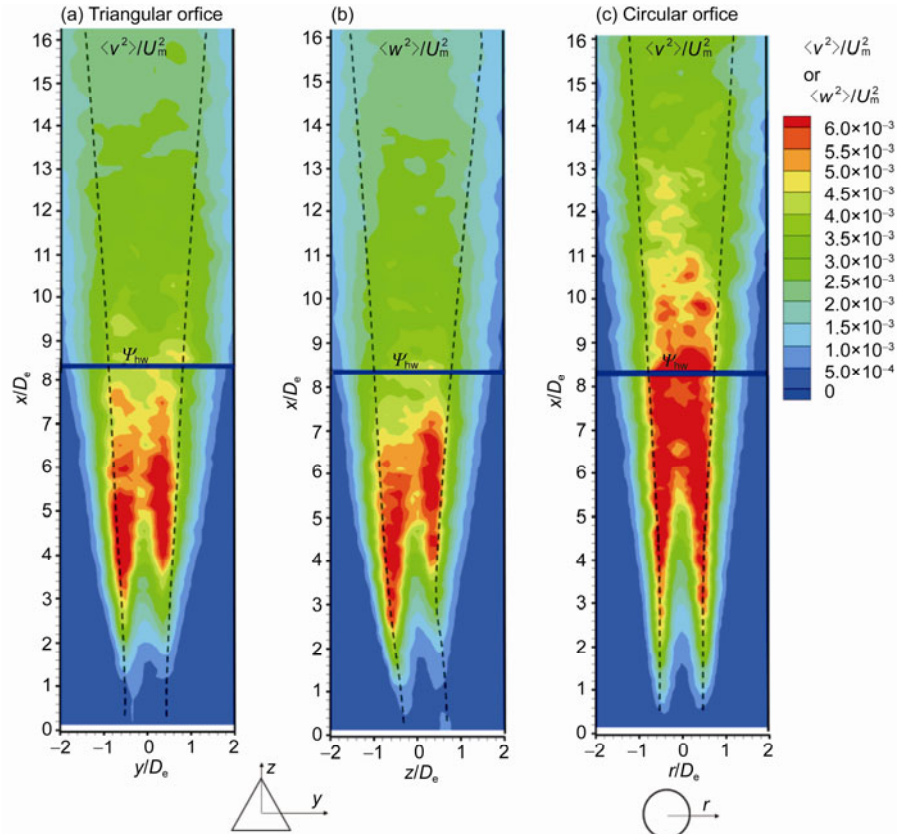
Figure 10 Contours of the lateral components of the normal stress ($\langle v^2 \rangle / U_m^2$ or $\langle w^2 \rangle / U_m^2$) in (a) and (b) the *x-y* and *x-z* planes of the triangular jet and (c) the central plane of the circular jet.
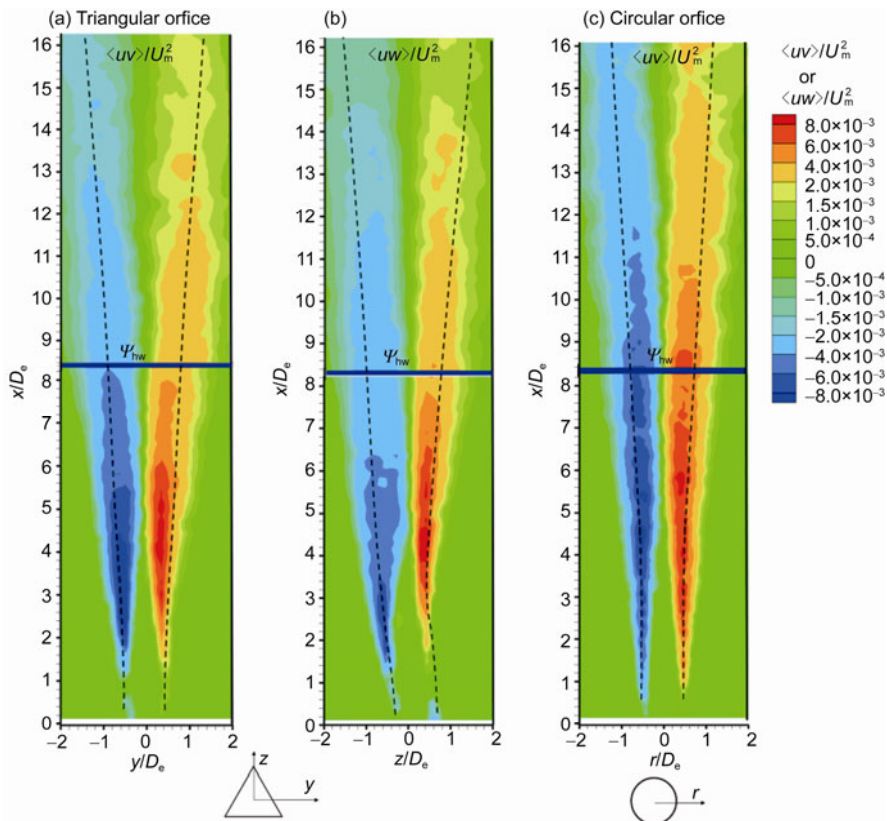
Figure 11 Contours of normalised Reynolds shear stresses ($\langle uv \rangle / U_m^2$ and $\langle uw \rangle / U_m^2$) in (a) and (b) the *x-y* and *x-z* planes of the triangular jet and (c) the central plane of the circular jet.

and then decay more rapidly than those of the circular jet. This is consistent with the observations of shorter "unmixed core" and faster decay rate above.

To quantitatively compare the evolution of the fluctuating velocity field, the streamwise turbulent intensity u'/U_c is presented in Figure 12. Also, results from Mi and Nathan [9] and Quinn [7] are added. Apparently, the turbulent intensity of the triangular jet increases more rapidly until $x/D_e \approx 5$, which indicates a higher rate of mixing with ambient fluid and scatters at $u'/U_c \approx 0.18$. By comparison, the transition position of the turbulent intensity moves downstream at $x/D_e \approx 10$ in the circular jet. Although the centreline turbulent intensity of the triangular jet increases more rapidly, the magnitude at the transition region is 25% smaller than that in the circular jet. Moreover, the centreline turbulent intensity of the circular jet remains at a higher value at $x/D_e > 10$. This observation is consistent in that there are more three-dimensional vortical structures in the triangular jet than that in the circular jet. In addition, it can be noted that the transition position of u'/U_c also occurs at $x/D_e \approx 5$ for Mi and Nathan [9] and Quinn [7], while u'/U_c is greater than the present result and still slowly increases as the flow developing downstream. This indicates, for Mi and Nathan [9] and Quinn [7], that the fluctuating velocity field of the triangular jets does not reach self-similarity at $x/D_e < 20$. The RMS velocity profiles of the present triangular jet are far from convergence in the entire measurement range, as their profiles in both the x-y plane and the x-z plane significantly retain differences at $x/D_e = 15$ (not shown here).

4   Conclusions

Herein we have investigated an equilateral triangular free jet
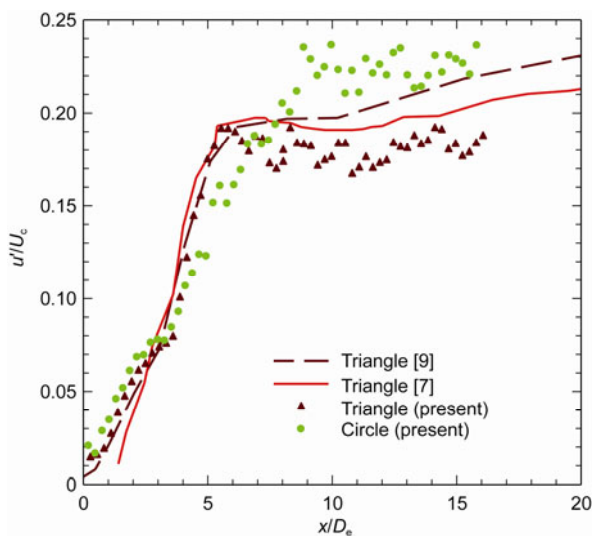
in the near and transition regions at Re=50,000 using a planar PIV technique. Comparison have been made for the-instantaneous, mean and turbulence velocity fields of two jets which issue from triangular and circular orifice plates, respectively. Based on the results reported in the present paper, several main conclusions can be made.

Firstly, the triangular jet entrains with the ambient fluid at a higher rate than the circular jet in the near and transition region. This is reflected by the higher spread and decay rates, more rapidly increasing centreline turbulent intensity, and shorter unmixed core.

Secondly, the triangular corner can induce small-scale vortical structures, while the flat side promotes large-scale structures, thus the primary vortical structures in the triangular jet has higher three-dimensionality than in the circular jet.

Thirdly, the "axis-switching" phenomenon is observed to occur in the present triangular jet at $x \approx 1.7 D_e$. Such phenomenon is believed to have a critical role to increase three-dimensionality of vortical structures and entrainment with ambient fluid.

Fourthly, although the self-preserving relations of the centreline mean velocity and half-velocity width appear to be met at $x/D_e \geqslant 10$ in the circular jet, the mean flow of the triangular jet is far from reaching self-similarity over the entire measurement region.

Fifthly, in the near field region, all components of Reynolds stress of the triangular jet appear to reach the peaks earlier, and then decay more rapidly than those of the circular jet.

Lastly, the turbulent intensity of the triangular jet increases more rapidly until $x/D_e \approx 5$ and then scatters at $u'/U_c \approx 0.18$ at $x/D_e > 5$. By comparison, the transition position of the turbulent intensity in the circular jet moves downstream at $x/D_e \approx 10$ and $u'/U_c \approx 0.23$ at $x/D_e > 10$.

1   Gutmark E, Grinstein F. Flow control with noncircular jets. Annu Rev Fluid Mech, 1999, 31(1): 239–272

2   Zaman K B M Q. Axis switching and spreading of an asymmetric jet: The role of coherent structure dynamics. J Fluid Mech Digital Archive, 1996, 316(1): 1–27

3   Gutmark E, Schadow K, Parr T, et al. Noncircular jets in combustion systems. Expt Fluids, 1989, 7(4): 248–258

4   Koshigoe S, Gutmark E, SCHADOW K, et al. Initial development of noncircular jets leading to axis switching. AIAA J, 1989, 27: 411–419

5   Grinstein F, Gutmark E, Parr T. Near field dynamics of subsonic free square jets: A computational and experimental study. Phys Fluids, 1995, 7(6): 1483–1497

6   Miller R, Madnia C, Givi P. Numerical simulation of non-circular jets. Compt Fluids, 1995, 24(1): 1–25

Figure 12   (Color online) Variations of the turbulent intensity u'/U_c along the jet centreline.

7 Quinn W. Mean flow and turbulence measurements in a triangular turbulent free jet. Int J Heat Fluid Fl, 1990, 11(3): 220–224

8 Quinn W. Measurements in the near flow field of an isosceles triangular turbulent free jet. Expt Fluids, 2005, 39(1): 111–126

9 Mi J, Nathan G. Statistical properties of turbulent free jets issuing from nine differently-shaped nozzles. Flow Turbul Combust, 2010, 84(4): 583–606

10 Iyogun C, Birouk M. Effect of sudden expansion on entrainment and spreading rates of a jet issuing from asymmetric nozzles. Flow Turbul Combust, 2009, 82(3): 287–315

11 Mi J, Kalt P, Nathan G J, et al. PIV measurements of a turbulent jet issuing from round sharp-edged plate. Expt Fluids, 2007, 42(4): 625–637

12 Bruun H H. Hot-wire Anemometry, Principles and Data Analysis. Oxford: Oxford University Press, 1994

13 Mi J, Xu M, Du C. Digital filter for hot-wire measurements of small-scale turbulence properties. Meas Sci Technol, 2011, 22: 125401

14 Xu M, Du C, Mi J. Centerline statistics of the small-scale trubulence of a circular jet and their dependence on high frequency noise. Acta Phy Sin, 2011, 60(3): 345353

15 He L, Yi S H, Zhao Y X, et al. Experimental study of a supersonic turbulent boundary layer using PIV. Sci China-Phys Mech Astron, 2012, 54(9): 1702–1709

16 Yang S Q, Jiang N. Tomographic TR-PIV measurement of coherent structure spatial topology utilizing an improved quadrant splitting method. Sci China-Phys Mech Astron, 2012, 55(10): 1863–1872

17 Pan C, Wang J J, Zhang C. Identification of Lagrangian coherent structures in the turbulent boundary layer. Sci China Ser G-Phys Mech Astron, 2009, 52(2): 248–257

18 Tang Z Q, Jiang N. Dynamic mode decomposition of hairpin vortices generated by a hemisphere protuberance. Sci China-Phys Mech As-

tron, 2012, 55(1): 118–124

19 Liu Z F, Wang L Z, Fu S. Study of flow induced by sine wave and saw tooth plasma actuators. Sci China-Phys Mech Astron, 2012, 54(11): 2033–2039

20 Mi J, Kalt P, Nathan G. On Turbulent jets issuing from notched-rectangular and circular orifice plates. Flow Turbul Combust, 2010, 84(4): 565–582

21 Xu M, Zhang J, Mi J, et al. Mean and fluctuating velocity fields of a diamond turbulent jet. Chin Phys B, 2013, 22(3): 034701

22 Hussain A, Clark A. On the coherent structure of the axisymmetric mixing layer: A flow-visualization study. J Fluid Mech, 1981, 104: 263–294

23 Schadow K, Gutmark E, Parr D, et al. Selective control of flow coherence in triangular jets. Expt Fluids, 1988, 6(2): 129–135

24 Ho C, Gutmark E. Vortex induction and mass entrainment in a small-aspect-ratio elliptic jet. J Fluid Mech, 1987, 179: 383–405

25 Hussain F, Husain H. Elliptic jets, Part 1. Characteristics of unexcited and excited jets. J Fluid Mech, 1989, 208: 257–320

26 Husain H, Hussain A. Controlled excitation of elliptic jets. Phys Fluids, 1983, 26: 2763–2765

27 Du C, Xu M, Mi J. Effect of exit Reynolds number on a turbulent round jet. Acta Phy Sin, 2010, 59(9): 6323–6330

28 Deo R C, Mi J, Nathan G J. The influence of Reynolds number on a plane jet. Phys Fluids, 2008, 20(7): 075108

29 Xu M, Pollard A, Mi J, et al. Effects of Reynolds number on some properties of a turbulent jet from a long square pipe. Phys Fluids, 2013, 25: 035102

30 Widnall S E. The structure and dynamics of vortex filaments. Annu Rev Fluid Mech, 1975, 7(1): 141–165

31 Hussein H, Capp S, George W. Velocity measurements in a high-Reynolds-number, momentum-conserving, axisymmetric, turbulent jet. J Fluid Mech, 1994, 258: 31–75